High-resolution measurement of the ${}^{12}C(\gamma,p){}^{11}B$ reaction to excited states for $E_\gamma = 50-70$ MeV

A. Kuzin, R. P. Rassool, and M. N. Thompson
The School of Physics, The University of Melbourne, Parkville 3052, Victoria, Australia

J.-O. Adler, K. Fissum, K. Hansen, L. Isaksson, M. Lundin, B. Nilsson, H. Ruijter, and B. Schröder
Department of Nuclear Physics, University of Lund, Sölvegaten 14, S-223 62 Lund, Sweden

J. R. M. Annand, G. I. Crawford, J. C. McGeorge, and J. Gregel
Department of Physics and Astronomy, University of Glasgow, Glasgow, G12 8QQ Scotland

J. Ryckebusch
Department of Subatomic and Radiation Physics, University of Gent, Proeftuinstraat 86, B-9000, Gent, Belgium
(Received 15 May 1998)

Relative population of states in ^{11}B following the ${}^{12}C(\gamma,p)$ reaction has been measured with high resolution using the deexcitation γ-ray technique. The states near 7 MeV in ^{11}B are clearly resolved and the measured population clarifies earlier conflicting data. Comparison of the results with new calculations indicates the importance of both one-nucleon and multinucleon processes. [S0556-2813(98)00410-5]

I. INTRODUCTION

For photonuclear reactions in the intermediate energy region, several different models have been used to describe the transition process between the initial $|i\rangle$ and final $|f\rangle$ nuclear states induced by photoabsorption. These models fall roughly into three categories: the direct knockout model (DKO), the quasideuteron models (QD), and microscopic models.

One argument in favor of DKO has been the scaling of the (γ,p) data with the missing momentum p_m [1,2]. Recently Owens *et al.* [3] have shown that scaling is consistent with processes that involve both one- and two-nucleon components, and thus does not necessarily validate the DKO model. An argument against the DKO derives from the large momentum mismatch between the incoming photon and the outgoing nucleon in this model. This leads to a small cross section resulting from the small high momentum components in the initial bound state wave function. The near equality of the experimental (γ,p) and (γ,n) cross sections is a natural consequence of the QD model, but is hard to explain in the DKO framework (because the neutron current is much smaller than the proton current). Although final state interactions modify the simplest DKO predictions, distorted wave impulse approximation (DWIA) calculations [4–6] are unable to give a consistent description of both (γ,p) and (γ,n) cross sections. In the more sophisticated microscopic models [7–9] a formal description of the concepts of the QD models are introduced in an attempt to include shell model contributions, nucleonic long-range correlations, and meson exchange currents in a consistent manner.

Recently it has also been shown [10] that relativistic calculations provide a fair description of the experimental (γ,p) data to states with a predominant $1h$ character for missing momenta below ~ 500 MeV/c. This might indicate that the meson exchange contributions are not large when the mean-field properties are treated in a relativistic framework.

With improved experimental techniques it became possible to determine the exclusive photoproton and photoneutron cross sections to specific groups of final states; but it was only possible to determine the cross sections for population of individual residual states in a few cases, where the states are well separated. For example in the most recent experiments [11–14] on the ${}^{12}C(\gamma,p){}^{11}B$ reaction, only the ground state and the first excited state were clearly resolved.

Following the ${}^{12}C(\gamma,p){}^{11}B$ reaction, the residual nucleus of ^{11}B can be left in an excited state. The level scheme of ^{11}B up to 8 MeV is shown in Fig. 1. Of particular interest are the three states near 7 MeV. These states all are predominantly $2h$-$1p$ in nature with the two holes in the $1p_{3/2}$ shell, but each has the neutron in a different orbit. The dominant configurations are [15,16] $|1p_{1/2}(1p_{3/2})^{-2}\rangle$ for the $\frac{7}{2}^-$ (6.74 MeV) state, $|2s_{1/2}(1p_{3/2})^{-2}\rangle$ for the $\frac{1}{2}^+$ (6.79 MeV) state,
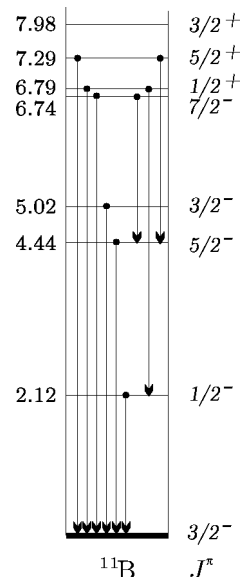

FIG. 1. Level structure in ^{11}B.

and $|1d_{5/2}(1p_{3/2})^{-2}\rangle$ for the $\frac{5}{2}^+$ (7.29 MeV) state. They may also be considered as a particle coupled to a core of ^{10}B in its ground state or in an excited state [17,18].

Experiments have, so far, failed to adequately determine the relative population of these three states near 7 MeV, which leads to ambiguity in interpretation of the data. For example, Van Hoorebeke *et al.* [13] concluded that the main strength near 7 MeV belongs to 7.29 MeV state, while Ruijter *et al.* [14] reported that the unresolved doublet at 6.8 MeV is dominant. All of the most recent measurements achieved a resolution no better than 450–700 keV [11–14], so that it was not possible to unambiguously measure the population even of the state at 7.29 MeV, since it is not resolved from the two states near 6.8 MeV. It is nearly impossible to resolve the latter two states at 6.8 MeV in a single-arm experiment, because their energy separation is only 50 keV. It is evident that in order to obtain more definitive results, better resolution is required, or a new experimental technique must be applied.

One possibility involves detection of the deexcitation γ rays from the decay of the excited states in the residual nucleus, as a measure of their population following the (γ,p) reaction. In this case even if the resolution for the protons is poor, the better resolution associated with the γ-ray detector, and particularly the observation of cascade γ-ray decays, can allow separation of the different residual states. The γ-ray detection reduces the count rate but, because the resolution is determined by the γ-ray detector, this can be partly offset by using a thicker target than in conventional (γ,p) experiments. However, it is important that the proton resolution is adequate to determine the excitation region in the residual nucleus associated with a particular deexcitation γ ray. Our preliminary analysis [19] of the present experiment showed that this new technique is practical for the ^{12}C(γ,p) reaction, and that the population of the 7.29 MeV state is considerably weaker than the states at 6.8 MeV. Here we give the results of a more sophisticated analysis which confirms the previous conclusion and leads to quantitative results for all states below 7.5 MeV in ^{11}B.

II. EXPERIMENTAL APPARATUS

The goal of the experiment was a measurement of the ^{12}C$(\gamma,p\gamma')^{11}$B reaction with the aim of investigating the population of the excited states in ^{11}B, particularly near 7 MeV. The experiment was performed at the tagged photon facility at the MAX lab, University of Lund.

A 95-MeV electron beam was incident on a 50-μm-thick Al radiator, producing a flux of bremsstrahlung photons. In the range from 50 to 70 MeV these photons were tagged using a magnetic spectrometer [20] equipped with two arrays of focal-plane detectors, each consisting of 32 plastic scintillators of individual width about 7 mm. This gave a photon energy resolution better than 300 keV. The beam of tagged photons was collimated to a diameter of ~ 2 cm at the graphite-carbon target with the dimensions of 10×10 cm, 2-mm thick (235 mg cm^{-2}). The target was placed at 25° to the beam as shown in Fig. 2.

Two of the three proton telescopes were placed above the target at a distance of 15 cm from its center, at angles of 70° and 125°. These two proton telescopes were based on 7.5-
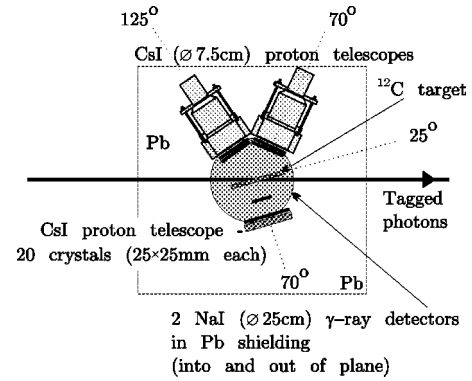

FIG. 2. Schematic layout of the experimental setup.

cm-diameter by 7.5-cm-deep CsI crystals coupled to photomultiplier tubes giving an intrinsic resolution of about 1% [21] (300–500 keV for 30–50 MeV protons). Each telescope was equipped with three semioverlapping 0.5-mm-thick NE102 plastic ΔE detectors. The third proton telescope, with an overall area of 10×12.5 cm, was placed at an angle of 70° below the target at a distance of 15 cm from its center. It was based on an array of the CsI crystals, each of size $25 \times 25 \times 30$ mm read out by photodiodes [22]. The intrinsic resolution of a single crystal element was measured as ~ 300 keV for proton energies of ~ 45 MeV.

The deexcitation γ-ray arm consisted of two 25-cm-diameter, 30-cm-deep NaI detectors. These were shielded by 10 cm of Pb with a collimator window of 15 cm in diameter, and were placed on either side of the target at a distance of 20 cm. The resolution of both NaI detectors varied from 140 to 270 keV for γ-ray energies from 2 to 6.3 MeV.

The total experimental proton energy resolution, determined mostly by the target thickness, was estimated to be between 2 and 2.6 MeV for the proton telescopes. This was adequate to determine the excitation region associated with a particular deexcitation γ ray.

The signals from the proton full-E and ΔE detectors, and the NaI detectors were fed into CAMAC ADC modules. The timing information from the tagger, ΔE, and NaI detectors was recorded in corresponding TDCs. A coincidence signal from a pair of ΔE detectors from any proton telescope triggered the electronics to provide a start pulse for all TDCs and a gate pulse for all ADCs, which initiated conversion in these modules. However, the final decision as to the acceptability of an event was determined by a requirement that signals from one CsI detector and the corresponding ΔE detector were coincident in time, and both exceeded preset thresholds. These threshold values were chosen using ΔE-E scatter plots for each proton telescope. Because of the shaping in the amplifiers this condition took 5–10 μs. If it was satisfied, readout of ADC and TDC modules was initiated; if not, the ADCs and TDCs were "fast cleared," thus greatly reducing the number of events triggered by electrons in the raw data.

III. DATA ANALYSIS AND RESULTS

A. Proton data analysis

For proton events the tagger TDC spectra exhibit three separate "prompt" peaks (one for each telescope) on a ran-
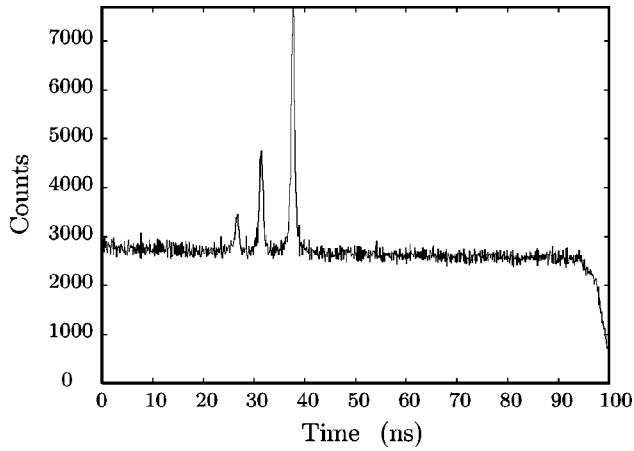
FIG. 3. Timing spectrum between signals from the three proton telescopes and the focal plane detectors (summed together). The peaks indicated are the prompt peaks.

dom background, see Fig. 3. The prompt timing region was determined for every TDC spectrum of each tagging electron detector. Using scatter plots of ΔE signals versus full-E signals for each proton telescope, proton events were separated from those triggered by electrons. For each tagged energy, peaks in the corresponding proton spectra were used to calibrate the ADCs.

For each proton detector the missing-energy spectrum for prompt events was generated. The missing energy is defined as $E_{\mathrm{miss}}=E_\gamma-T_p-T_R$, where T_R is the kinetic energy of the recoil nucleus ^{11}B, and T_p is the kinetic energy of the emitted proton. The excitation energy is related to the missing energy E_{miss}, as $E_{\mathrm{ex}}=E_{\mathrm{miss}}-Q$, where Q is the separation energy for the ^{12}C$(\gamma,p)^{11}$B reaction. The missing-energy spectra produced by photons of different tagged energy were summed to produce spectra with good statistics at angles of 70° and 125°.

The spectra for events in the prompt region of the proton-tagger time spectra also contained random background. This contribution was deduced using events whose timing was outside the prompt region in the tagger TDC spectra. The missing-energy spectrum at 70°, corrected for the random background, is presented in Fig. 4.

B. Deexcitation γ-ray spectra analysis

The deexcitation γ-ray spectra were produced by cutting on particular regions of the missing energy spectra. Such prompt deexcitation γ rays associated with selected protons all have the same timing relative to the protons, and were easily identified in a NaI TDC spectrum triggered by the protons. The requirement of a timing coincidence reduced the level of uncorrelated background γ rays. For ^{11}B, the region of particular interest is the excitation-energy region around 7 MeV, where the unresolved states form the broad bump seen in the missing-energy spectrum. The energy region from 5 to 9 MeV was therefore used to produce an associated deexcitation spectrum (labeled 5–9). This spectrum includes the cascade γ rays from the states near 7 MeV but not the direct decay of the 2.12 MeV state [23].

Since the 2.12 MeV state is the only excited state in ^{11}B below 4 MeV, the deexcitation γ-ray spectrum for events
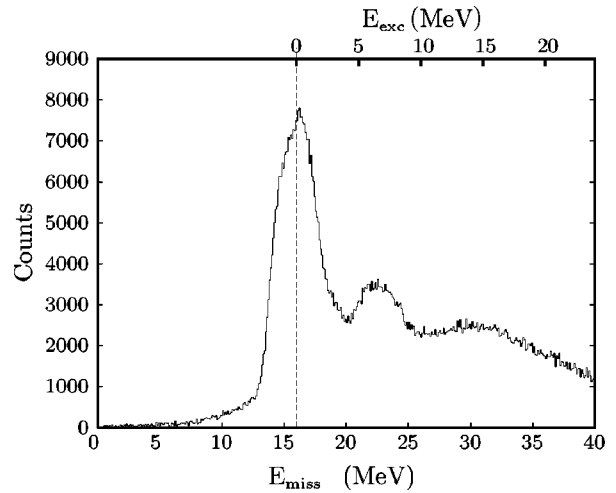

FIG. 4. The missing-energy spectrum for the ^{12}C$(\gamma,p)^{11}$B reaction ($\theta_p\sim70°$, $E_\gamma=50-70$ MeV) obtained for one of the CsI elements of the array detector. The excitation-energy scale is also shown on the upper axis. Background has been subtracted.

with excitation energy between 0 and 3 MeV (0–3 spectrum) should show only γ rays of this energy. The measured spectrum (see Fig. 5) indeed shows a strong peak at 2.12 MeV, while the 5–9 spectrum shows the presence of both 2.12 and 2.30 MeV cascade lines from the decay of 6.79 and 6.74 MeV states, respectively.

Several corrections were made to the 5–9 deexcitation γ-ray spectrum before it was unfolded. First, the γ-ray contribution resulting from the random-coincidence background proton data was subtracted from the prompt γ-ray spectrum, which reduced the number of counts by $\sim30\%$. Also the 5–9 spectrum was corrected for the presence of γ rays associated with photoproton reactions with the air ($\sim5-10\%$ contribution), and the presence of direct 2.12 MeV γ rays ($\sim10\%$) due to protons populating this state directly, but which are present in the 5–9 MeV missing-energy region because of relatively poor proton energy resolution.

To determine the relative strengths of the various γ rays in the experimental spectrum, it was necessary to allow for
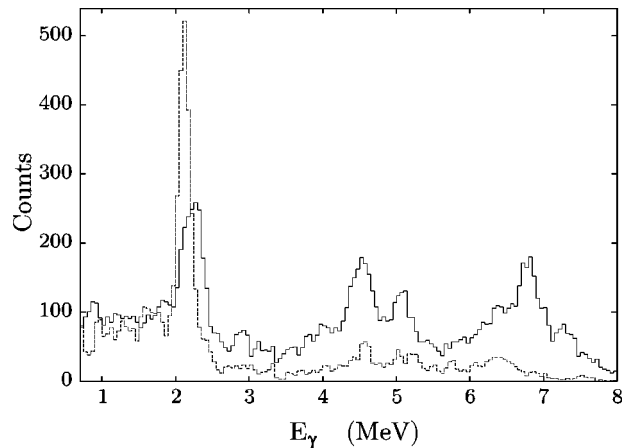

FIG. 5. Deexcitation γ-ray spectra for the ^{12}C$(\gamma,p)^{11}$B reaction ($E_\gamma=50-70$ MeV, $\theta_p\approx70°$) for events within 0–3 MeV (dashed line) and 5–9 MeV (solid line) regions of the ^{11}B excitation energy spectrum. These γ-ray spectra are referred to as 0–3 and 5–9 spectra.

the γ-ray detector response function (RFN). This was calculated for a number of γ-ray energies using the GEANT [24] software. Such a RFN comprised a full-energy peak, a single escape peak, a rather small double escape peak and Compton contribution (Compton ''tail''). The RFNs were parametrized as a function of energy. However, the calculated RFNs had to be modified to conform to the experimental situation. The experimental resolution for γ rays up to 5 MeV was determined from the spectra taken with radioactive sources. The deexcitation γ rays from sufficiently resolved states in ^{11}B at 5.02 and 7.29 MeV were used to estimate the resolution in the 5–7 MeV region. This experimental resolution was found to be $\sim 50\%$ worse than the calculated one, and the Compton contribution was found to be between 30 and 50 % larger than calculated for photon energies from between 2 and 7 MeV. This was partly due to adding γ-ray spectra from the two NaI detectors, both of which might have slight uncertainties in their calibration. The RFN was modified to reflect these experimental corrections.

The fit to the γ-ray spectrum was performed with the PAW [25] software. The fitting routine was optimized using the forward angle data with better statistics. After the fit and RFN parameters (such as exact peak positions, resolution, Compton contribution, single- and double-escape strengths, etc.) were adjusted by minimizing the χ^2 values of the fit, the only varying parameters were the heights of the full-energy peak. The fit was performed for spectra containing dependent γ lines, so self consistency of the data was maintained. This was achieved by knowing that the strength of the population of a given state must be the same, whether it is determined from the γ-ray decay strength direct to the ground state or the cascade γ-ray decay strength, using the known branching ratios [23] (see also Fig. 1). For the 5–9 spectrum this gives the following constraints: (i) The strength at 2.12 MeV is determined by the cascade decays from the 5.02 and 6.79 MeV states [i.e., the number of 2.12 MeV to ground state transitions (2.12-0) should be equal to the sum of 5.02-2.12 and 6.79-2.12 transitions], (ii) the strength at ~ 2.3 MeV is determined by the cascade decays from the 6.74 and 7.29 MeV states, (iii) the strength at ~ 2.90 MeV is determined by the cascade decays from 5.02 and 7.29 MeV states, (iv) the strength at ~ 4.5 MeV includes contributions at 4.67 MeV due to the cascade γ rays from the 6.79 MeV state, and from the 4.44 MeV cascade γ rays from the 6.74 MeV state. After accounting for these, the remaining strength is due to direct population of the 4.44 MeV state following the ^{12}C$(\gamma,p)^{11}$B reaction.

C. Results

1. Forward angle

The final corrected 5–9 deexcitation γ-ray spectrum from the 70° data was obtained from data from both forward angle telescopes and both NaI detectors, and it was unfolded using the response functions for all the γ lines mentioned above to produce the fit presented in Fig. 6. This confirms the preliminary result [19] that the population of the 7.29 MeV state is considerably weaker than the states at 6.9 MeV, knowing that these states decay predominantly to the ground state [23]. There seems to be an unaccounted peak below 2.12 MeV, however, there are no known sources of 1.9–2.0 MeV
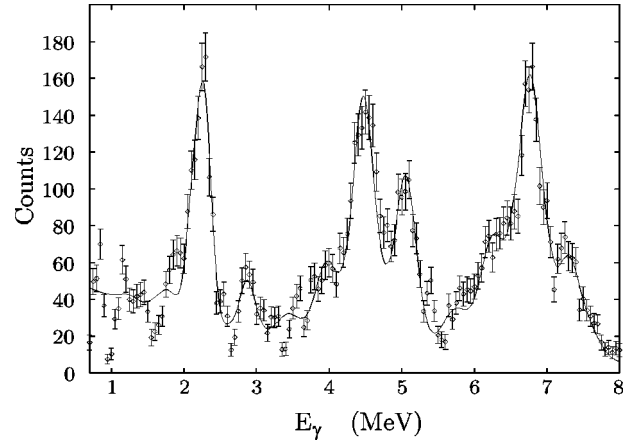

FIG. 6. Forward angle deexcitation 5–9 γ-ray spectrum fitted with the response functions (solid line).

γ rays from ^{11}B and no deexcitation γ rays with this energy from ^{10}B following a (γ,pn) reaction.

From the fit the number of counts included in each full-energy peak was determined. The relative population of the relevant states in ^{11}B was then determined using these numbers corrected for the energy-dependent efficiency of the NaI detectors calculated using the GEANT code and using the γ-ray branching ratios [23].

As a result of these procedures, it was possible to determine the relative strengths of the two states at 6.74 and 6.79 MeV; the major advance in the present work. The relative strength of these two states was used in the following final stage of the data analysis.

The deexcitation γ-ray spectrum derived from the region of 5–9 MeV of the excitation energy spectrum of ^{11}B, provided only the relative populations of the states near 7 MeV in ^{11}B. It was also necessary to obtain information about the population of the other states in ^{11}B, which was done using all (γ,p) events in the missing-energy spectrum from 0 to 11 MeV. No noticeable population of states above the 7.29 MeV state was observed. Since the relative strengths of the 6.74 and 6.79 MeV states were now known, the strength of the corresponding cascade γ-rays was deduced in order to correct for their contribution to the spectrum.

The results for the relative population of the states in ^{11}B following the ^{12}C$(\gamma,p)^{11}$B reaction at an angle of 70° are presented in Table I. The errors include statistical uncertainties, fitting errors, uncertainties in NaI detector efficiency, and uncertainties in the branching ratios.

TABLE I. Relative population of the states in ^{11}B following the ^{12}C$(\gamma,p)^{11}$B reaction ($E_\gamma = 50$–70 MeV, $\theta_p \approx 70°$).

Energy, MeV	J^π	Population p_i (arb. units)	$\dfrac{P_i}{P_{6.74}}$
2.12	$\frac{1}{2}^-$	8646 ± 400	0.89 ± 0.10
4.44	$\frac{5}{2}^-$	$<3691 \pm 400$	0.38 ± 0.06
5.02	$\frac{3}{2}^-$	8979 ± 400	0.92 ± 0.10
6.74	$\frac{7}{2}^-$	9726 ± 1000	1.00
6.79	$\frac{1}{2}^+$	2203 ± 200	0.23 ± 0.03
7.29	$\frac{5}{2}^+$	3398 ± 150	0.35 ± 0.05

2. Backward angle

A similar analysis was carried out on the de-excitation spectra recorded with the proton detector at 125°. The final deexcitation γ-ray spectrum is presented in Fig. 7.

The cross section for the $^{12}C(\gamma,p)^{11}B$ reaction depends strongly on the proton emission angle, decreasing with increasing angle. This angular dependence, and the use of only one proton detector at the backward angle, reduced the proton count rate significantly. The statistics are therefore significantly poorer than for the forward-angle data, but again the main features are clearly evident, and the relative strengths could be extracted, see Table II. Comparing Figs. 6 and 7 (and Tables I and II) it is quite evident that at the backward angle, the population of the 7.29 MeV state has dropped significantly, relative to the population of the doublet at 6.8 MeV. It may be noted that though the fit might be visibly improved by possibly reducing the intensity of the 6.8 MeV peak, this would probably make the fit worse around 5.8 MeV and definitely violate the constraints imposed by the decay schemes.

3. Cross sections

Although the present measurement gives the relative population of excited states in ^{11}B, including those resolved near 7 MeV, it does not allow the absolute cross sections to be obtained. Conversely, earlier measurement of the $^{12}C(\gamma,p)$ reaction, e.g., by Springham et al. [12] and Ruijter et al. [14] which failed to resolve the states near 7 MeV, were nonetheless able to assign absolute cross sections. It was thus possible to normalize the present results and derive an absolute cross section scale for all the observed states, including those at 7 MeV. This normalization used the average values of the cross sections from the measurements mentioned above [12,14]. The cross sections to the three states near 7 MeV are listed in Table III.

Table IV shows the cross sections to the states in ^{11}B at similar angles, as reported in all three experiments. To allow comparison the cross sections to the states near 7 MeV reported here have been added together. The overall consistency is good considering the errors and the differences in angles and photon energy bins.
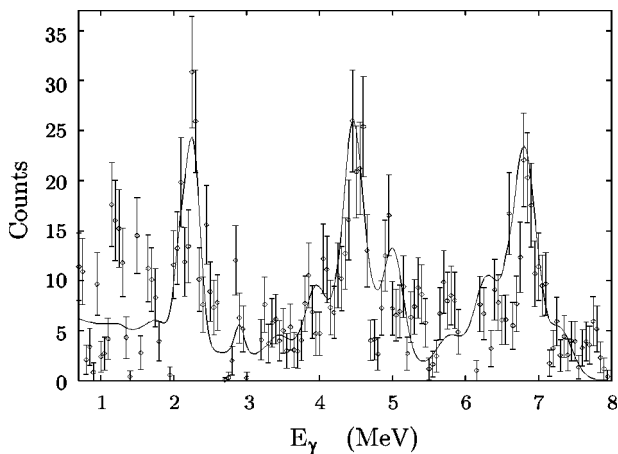

FIG. 7. The deexcitation 5–9 γ-ray spectrum at 125° fitted with the response functions (solid line).

TABLE II. Relative population of the states in ^{11}B following the $^{12}C(\gamma,p)^{11}B$ reaction ($E_\gamma = 50-70$ MeV, $\theta_p \approx 125°$).

Energy, MeV	J^π	Population P_i (arb. units)	$\dfrac{P_i}{P_{6.74}}$
2.12	$\frac{1}{2}^-$	404 ± 40	0.26 ± 0.06
4.44	$\frac{5}{2}^-$	$<780 \pm 90$	0.51 ± 0.11
5.02	$\frac{3}{2}^-$	1253 ± 120	0.82 ± 0.18
6.74	$\frac{7}{2}^-$	1526 ± 300	1.00
6.79	$\frac{1}{2}^+$	400 ± 120	0.26 ± 0.09
7.29	$\frac{5}{2}^+$	270 ± 30	0.18 ± 0.04

IV. DISCUSSION

As outlined in Sec. I, several modern theories exist which are used to calculate the cross sections to different residual states in photonuclear reactions. These theories have been evolving as new high quality data became available. Information as to which particular final state is populated, provides restrictions on the predictions of the models of the magnitude and angular distribution of these cross sections. However, in addition to final-state properties, the initial-state wave function is equally important in such calculations, since it provides the description of all the charges and currents in the nucleus.

Several groups [7,26,8,9,27] have ascribed a considerable fraction of the observed photoproton strength to multinucleon mechanisms that manifest themselves both in the photoabsorption (meson-exchange currents), and the final-state interaction (multistep or coupled-channel effects). In this paper the present results are compared with the calculations in the shell-model framework. Earlier Ryckebusch et al. [15] suggested that the relatively strong population of states with a $2h$-$1p$ character in the photoproton reactions was a proof for the importance of photoabsorption on meson exchange currents. It is worth remarking that the latter are predominantly of proton-neutron nature, so that the calculations [15] are essentially a microscopic formulation of the QD picture. Above the two-nucleon emission threshold, the dominant role of the meson exchange currents is a natural explanation for the dominance of the (γ,pn) channel in the total photoabsorption strength. Two-body currents naturally lead to excitation of states with a predominant $2h$-$1p$ character, even when a one-step reaction mechanism is considered. The early calculation of the differential cross section for the population of the states near 7 MeV [15] included two-body currents involving exchange of one pion only. This calculation also predicted that at forward angles, and for $E_\gamma \sim 60$ MeV, the $\frac{5}{2}^+$ (7.29 MeV) state would dominate,

TABLE III. Cross sections to the $\frac{7}{2}^-$ (6.74 MeV), $\frac{1}{2}^+$ (6.79 MeV), and $\frac{5}{2}^+$ (7.29 MeV) states in ^{11}B following the $^{12}C(\gamma,p)^{11}B$ reaction for $E_\gamma = 60$ MeV.

State	$\sigma(70°)$, μb/sr	$\sigma(125°)$, μb/sr
$\frac{7}{2}^-$ (6.74 MeV)	4.76 ± 0.82	2.25 ± 1.04
$\frac{1}{2}^+$ (6.79 MeV)	1.08 ± 0.19	0.59 ± 0.30
$\frac{5}{2}^+$ (7.29 MeV)	1.66 ± 0.29	0.40 ± 0.17

TABLE IV. Comparison of the present results from Tables I and II with the previous measurements of the $^{12}C(\gamma,p)^{11}B$ reaction (∗: corrected for the solid angle, see Sec. II for detectors setup).

Data	E_{ex}, MeV	$\sigma(\mu b/sr)_{fwd}$	θ_p	$\frac{\sigma(2.12)}{\sigma(\sim7)}$	$\sigma(\mu b/sr)_{bkwd}$	θ_p	$\frac{\sigma(2.12)}{\sigma(\sim7)}$	$\frac{\sigma(fwd)}{\sigma(bkwd)}$
HR [14]	2.12	6.84±0.72			0.66±0.22			10.4±3.6
			60°	0.79±0.11		120°	0.18±0.06	
$\overline{E}_\gamma=$ 59.7 MeV	~7	8.54±0.80			3.68±0.52			2.32±0.39
SPR [12]	2.12	5.1±0.5			0.8±0.8			6.4±6.4
			70°	0.78±0.11		115°	0.29±0.31	
$\overline{E}_\gamma=$ 59.7 MeV	~7	6.5±0.6			2.8±1.1			2.32±0.94
		(Populations P_i)			(Populations P_i)			
Present	2.12	8646±400			404±40			5.86±0.64*
			70°	0.56±0.05		125°	0.18±0.04	
$\overline{E}_\gamma=$ 60 MeV	Σ7	15327±1300			2196±450			1.9±0.42*

while the $\frac{7}{2}^-$ (6.74 MeV) would become dominant only for $\theta > 120°$. It also predicted that the $\frac{1}{2}^+$ (6.79 MeV) state would not contribute significantly to the strength around 7 MeV. The results of these calculations agreed well with the data by Springham *et al.* [12] where the limited experimental resolution did not allow the relative population of the individual states near 7 MeV to be determined.

The present results clearly indicate that population of the $\frac{7}{2}^-$ (6.74 MeV) state dominates over that of the positive parity states at both forward and backward angles (see previous section). This contrasts with the theoretical prediction [15] that the $\frac{5}{2}^+$ (7.29 MeV) state is dominant at forward angles. The present data also show that while the relative strength of the $\frac{1}{2}^+$ (6.79 MeV) state compared to the strength of the $\frac{7}{2}^-$ (6.74 MeV) state remains approximately the same at forward and backward angles, the relative population of the $\frac{5}{2}^+$ (7.29 MeV) state is significantly reduced at 120° implying a quite different angular dependence.

The superior resolution of the present experiment makes it clear that the assumptions which were at the basis of the calculations of Ryckebusch *et al.* [15] needed to be reconsidered. The calculation presented here is based on the same assumptions as far as the excitation of the $2h$-$1p$ components in the final state is concerned. However, two important additions were made. First, Δ currents were added to the two-body part of the nuclear current operator. The effect of those, however, was found to be relatively small for the photon energies considered here. Second, it was observed that quasielastic $^{12}C(e,e'p)$ measurements pointed towards small but measurable single-hole components for each of the states near 7 MeV [28]. This was interpreted as direct evidence for the existence of ground-state correlations in ^{12}C, and for the occupation of the $1f_{7/2}$ ($\frac{7}{2}^-$), $1d_{5/2}$ ($\frac{5}{2}^+$), and $2s_{1/2}$ ($\frac{1}{2}^+$) single-particle orbits in the ground state: these orbits would remain unoccupied in an independent-particle picture.

For the revised calculations presented here, the single-hole component in the $\frac{7}{2}^-$, $\frac{5}{2}^+$, and $\frac{1}{2}^+$ states was considered. The corresponding spectroscopic factors were taken from the $^{12}C(e,e'p)$ measurements reported by van der Steenhoven *et al.* [28]. These spectroscopic factors are 0.017 $(1d_{5/2}, \frac{5}{2}^+)$, 0.010 $(2s_{1/2}, \frac{1}{2}^+)$, and 0.0038 $(1f_{7/2}, \frac{7}{2}^-)$.

In spite of the small values of the spectroscopic factors for the single-hole components in the predominantly $2h$-$1p$ states, the most significant conclusion was that the one-body component was important, since the two-body components interfere (destructively or constructively) with the one-body term. Note that both one-body and two-body currents can excite the single-hole components in the final state, and that both contributions were considered in calculations. As a matter of fact, after including the one-body term the total predicted strength for the states near 7 MeV was not very much affected, the major effect of the one-hole components being redistribution of the strength over the different states.

The outlined additions appear to be quite important, since after including the single-hole component, the calculations predict the relative strengths of population of the states near 7 MeV to be in quite good agreement with the present data. The cross sections to the three states near 7 MeV in ^{11}B as

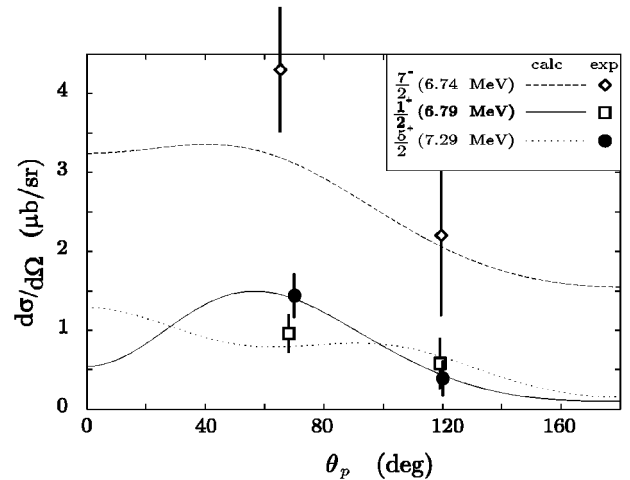FIG. 8. Differential (γ,p) cross sections at $\overline{E}_\gamma=60$ MeV for population of the three states near 7 MeV in ^{11}B after including both $1h$ and $2h$-$1p$ components in the final state. The calculations include one-body, pion-exchange, and Δ currents.

calculated, are presented in Fig. 8 together with the experimental values.

It is evident that these calculations correctly predict the dominance of the $\frac{7}{2}^-$ (6.74 MeV) state over the two positive parity states. Considering the experimental errors, especially at backward angles, and the fact that the theoretical curves involve a number of interfering mechanisms, the agreement with the experimental data is reasonable. We conclude that the basic premises of the calculations model the reaction reasonably well.

V. CONCLUSIONS

The present data provide the first reliable estimates of the population strengths of the three states near 7 MeV in ^{11}B following the ^{12}C$(\gamma,p)^{11}$B reaction. This in turn has prompted an improved calculation involving a more realistic picture of the reaction.

The ^{12}C(γ,p) calculations used the same procedure adopted earlier for the excitation of the positive parity states in ^{16}O(γ,p) [29]. Both the excitation of the states near 7 MeV in ^{11}B and the $(\frac{1}{2}^+,\frac{5}{2}^+)$ positive parity states in ^{15}N could be reasonably described by considering a coherent mixing of the small $1h$ and large $2h$-$1p$ components. The amplitude for the $1h$ components are constrained by the $(e,e'p)$ spectroscopic factors. For the "spectroscopic factors" corresponding to the $2h$-$1p$ components in the final wave function [that are almost unexcited in quasielastic $(e,e'p)$ reaction] one has to rely on shell-model calculations. The strong excitation of the $(\frac{1}{2}^+,\frac{5}{2}^+)$ doublet in ^{15}N

and the three states near 7 MeV in ^{11}B in (γ,p) reactions points towards occupation of $2h$-$1p$ states that would be unoccupied in an independent-particle model [confirming the $(e,e'p)$ results] and a substantial role for the meson-exchange currents (or multinucleon effects) in (γ,p) reactions (as this is the mechanism that can excite the $2h$-$1p$ components).

All of these dynamic ingredients were necessary in order to reach a reasonable description of the cross section to the different residual states. Considering the complexity of the interaction of a photon with nucleons and nuclear currents in a complex nuclei, this microscopic calculation gives a reasonable account of the data.

The deexcitation γ-ray technique used in photonuclear physics has advanced the quality of the experimental ^{12}C$(\gamma,p)^{11}$B data. This technique is going to be utilized in future (γ,p), (γ,n), and (γ,pn) experiments to provide improved resolution and complementary information to further constrain theoretical calculations.

[1] D. J. S. Findlay and R. O. Owens, Nucl. Phys. **A292**, 53 (1977).

[2] D. J. S. Findlay et al., Phys. Lett. **74B**, 305 (1978).

[3] R. O. Owens, J. L. Matthews, and G. S. Adams, J. Phys. G **17**, 261 (1991).

[4] S. Boffi, C. Giusti, and F. D. Pacati, Nucl. Phys. **A359**, 91 (1981).

[5] S. Boffi, R. Cenni, C. Giusti, and F. D. Pacati, Nucl. Phys. **A420**, 38 (1984).

[6] S. Boffi, F. Capuzzi, C. Giusti, and F. D. Pacati, Nucl. Phys. **A436**, 438 (1985).

[7] M. Gari and H. Hebach, Phys. Rep. **72**, 1 (1981).

[8] M. Cavinato, M. Marangoni, and A. M. Saruis, Nucl. Phys. **A422**, 237 (1984).

[9] J. Ryckebusch, M. Waroquier, K. Heyde, and D. Ryckbosch, Nucl. Phys. **A476**, 237 (1988).

[10] J. I. Johansson and H. S. Sherif, Phys. Rev. C **56**, 328 (1997).

[11] A. C. Shotter et al., Phys. Rev. C **37**, 1354 (1988).

[12] S. Springham et al., Nucl. Phys. **A517**, 93 (1990).

[13] L. van Hoorebeke et al., Phys. Rev. C **42**, R1179 (1990).

[14] H. Ruijter et al., Phys. Rev. C **54**, 3076 (1996).

[15] J. Ryckebusch et al., Phys. Rev. C **46**, R829 (1992).

[16] P. D. Harty et al., Phys. Rev. C **51**, 1982 (1995).

[17] J. W. Olness, Phys. Rev. **139**, B512 (1965).

[18] W. D. Teeters and D. Kurath, Nucl. Phys. **A275**, 61 (1977).

[19] A. Kuzin et al., Aust. J. Phys. **49**, 1075 (1996).

[20] J.-O. Adler et al., Nucl. Instrum. Methods Phys. Res. A **388**, 17 (1997).

[21] D. A. Sims, Internal report, University of Melbourne (unpublished).

[22] J. Annand et al., Nucl. Instrum. Methods Phys. Res. A **292**, 129 (1990).

[23] F. Ajzenberg-Selove, Nucl. Phys. **A506**, 1 (1990).

[24] GEANT Detector Description and Simulation Tool, CERN, Geneva, 1993.

[25] PAW Physics Analysis Workstation, CERN Program Library Q121, 1993.

[26] M. Cavinato, M. Marangoni, P. L. Ottaviani, and A. M. Saruis, Nucl. Phys. **A373**, 445 (1982).

[27] T. B. Bright and S. R. Cotanch, Phys. Rev. Lett. **71**, 2563 (1993).

[28] G. van der Steenhoven et al., Nucl. Phys. **A484**, 445 (1988).

[29] G. Miller et al., Nucl. Phys. **A586**, 125 (1995).